Published in final edited form as:

Cancer Res. 2023 February 15; 83(4): 553–567. doi:10.1158/0008-5472.CAN-22-1638.

Sphingosine kinase 2 in stromal fibroblasts creates a hospitable tumor microenvironment in breast cancer

Cynthia Weigel[1,*], **Melissa A. Maczis**[1,*], **Elisa N. D. Palladino**[1], **Christopher D. Green**[1], **Michael Maceyka**[1], **Chunqing Guo**[2], **Xiang-Yang Wang**[2], **Mikhail G. Dozmorov**[3], **Sheldon Milstien**[1], **Sarah Spiegel**[1]

[1]Department of Biochemistry and Molecular Biology and the Massey Cancer Center, Virginia Commonwealth University School of Medicine, Richmond, VA 23298

[2]Department of Human and Molecular Genetics, Virginia Commonwealth University School of Medicine, Richmond, VA 23298

[3]Departments of Biostatistics and Pathology, Virginia Commonwealth University School of Medicine, Richmond, VA 23298

Abstract

Reciprocal interactions between breast cancer cells and the tumor microenvironment are important for cancer progression and metastasis. We report here that the deletion or inhibition of sphingosine kinase 2 (SphK2), which produces sphingosine-1-phosphate (S1P), markedly suppresses syngeneic breast tumor growth and lung metastasis in mice by creating a hostile microenvironment for tumor growth and invasion. SphK2 deficiency decreased S1P and concomitantly increased ceramides, including C16-ceramide, in stromal fibroblasts. Ceramide accumulation suppressed activation of cancer-associated fibroblasts (CAFs) by upregulating stromal p53, which restrained production of tumor-promoting factors to reprogram the tumor microenvironment and restrict breast cancer establishment. Ablation of p53 in SphK2-deficient fibroblasts reversed these effects, enabled CAF activation and promoted tumor growth and invasion. These data uncovered a novel role of SphK2 in regulating non-cell autonomous functions of p53 in stromal fibroblasts and their transition to tumor-promoting CAFs, paving the way for the development of a strategy to target the tumor microenvironment and enhance therapeutic efficacy.

Correspondence to Sarah Spiegel, Department of Biochemistry and Molecular Biology, 2-011 Sanger Hall, Virginia Commonwealth University School of Medicine, 1101 E. Marshall Street, Richmond, VA 23298, Phone: 804-828-9330, sarah.spiegel@vcuhealth.org.
*These authors contributed equally to this work.

Authors' Contributions

C.W. and M.A.M. designed and performed the experiments and analyzed the data; C.W. performed confocal microscopy and experiments with primary cells, animals, and FACS; E.P. and M.M. performed p53 staining and confocal microscopy; M.D. analyzed RNA-seq data; C.G. and X.-Y.W. helped with FACS analyses; C.D.G. maintained colonies and performed QPCR; S.M. provided advice, helped with data analysis, and edited the manuscript. S.S. supervised the study, designed the experiments, analyzed the data, and wrote the manuscript.

Competing Interests: The authors declare no conflict of interest.

Additional Information

Supplementary Materials accompanies this paper.

Keywords

metastasis; triple-negative breast cancer; sphingosine kinase 2; ceramide; p53; anti-cancer immunity; cancer associated fibroblasts; tumor microenvironment

INTRODUCTION

Breast cancer is one of the most common malignant diseases in women. Most breast cancer-related deaths are not caused by the primary tumor itself, but are due to metastasis with a poor survival rate that has not changed much over the past 30–40 years. However, the molecular mechanisms underlying breast cancer metastasis have not yet been completely elucidated. The triple-negative breast cancer (TNBC) subtype, characterized by the absence of the estrogen receptor (ER), progesterone receptor (PR), and human epidermal growth factor receptor 2 (HER2), is aggressive with high recurrence, metastasis, and mortality rates. The inability to effectively predict, prevent, and treat metastatic breast cancer is a major problem in breast cancer care, and the development of additional effective targeted therapies is urgently required (1). It is well known that reciprocal interactions between cancer cells and the tumor microenvironment composed of the extracellular matrix and various cell types, including immune cells, fibroblasts, and endothelial cells, are important for disease progression, metastasis, and prognosis (2). The tumor microenvironment continually changes throughout cancer progression, underscoring the need for a better understanding of the cellular and molecular mechanisms governing tumor-stroma interactions that could initiate the development of additional effective treatments to suppress breast cancer progression, metastasis, and recurrence (3).

Sphingosine-1-phosphate (S1P) is a pleiotropic bioactive sphingolipid metabolite that regulates numerous fundamental biological processes important for breast cancer progression and metastasis, including cell growth and survival, motility, invasion, and immune cell trafficking (4). S1P is produced intracellularly from sphingosine, the backbone of sphingolipids, by two closely related sphingosine kinases SphK1 and SphK2. It is exported out of cells by specific transporters and exerts many of its effects via the activation of specific cell surface S1P receptors (4). There is abundant evidence linking SphK1 to breast cancer (5,6). SphK1 expression is elevated in patients with breast cancer and correlates with poor prognosis and chemotherapy resistance (5). Moreover, increased circulating levels of S1P produced by tumor SphK1 in mice prime distant pre-metastatic niches and are correlated with breast cancer progression and pulmonary metastasis (6). Nevertheless, it has been suggested that cancer cells communicate with the host organism to regulate lung colonization and metastasis via S1P generated systemically by SphK1, rather than by the tumor (7). As nothing is yet known about such a role for SphK2, and previous studies have suggested that increasing circulating S1P leads to increased metastasis, we examined the effect of deletion of endogenous SphK2 on syngeneic breast tumor growth and lung metastasis. Our study uncovered a previously unappreciated role of SphK2 in regulating tumor suppressor p53 in stromal fibroblasts involved in the activation of cancer-associated fibroblasts (CAF). Deletion or inhibition of SphK2 restrained the production of tumor-promoting factors, creating an active anti-tumor microenvironment. Targeting SphK2

in the stromal compartment may lead to the development of new therapeutic strategies that interfere with cancer progression and metastasis.

MATERIALS AND METHODS

Cell Culture

E0771.LMB (mCherry+) cells were obtained from Robin L. Anderson (University of Melbourne). E0771.luc cells were kindly provided by Paula D. Bos (Virginia Commonwealth University School of Medicine, Richmond, VA) (8). MMTV-Wnt-1 cells were derived from spontaneous mammary tumors from MMTV-Wnt-1 transgenic mice and were kindly provided by Emily J. Gallagher (School of Medicine at Mount Sinai, New York, NY). Mouse embryonic fibroblasts (MEFs) were isolated from E14 WT and SphK2$^{-/-}$ mouse embryos. Cells were cultured in DMEM (Gibco 4.5 g/L glucose, # 11960–044) supplemented with 10% FBS and pen/strep, sodium pyruvate, and GlutaMAX (Gibco, # 15140122, 11360070, 35050061). Primary human mammary fibroblasts isolated from normal human breast tissue from Cell Biologics (#H-6071) were cultured in complete fibroblast medium (CellBiologics, #M2267). Primary murine lung fibroblasts were cultured in fibroblast growth medium FM containing 2% FBS, 1% fibroblast growth supplement, and pen/strep (ScienCell, # 2301). Primary murine lung epithelial cells were cultured in epithelial cell medium (EpiCM-a, ScienCell, #4131) containing 2% FBS, 1% epithelial cell growth supplement-animal (EpiCGS-a), and pen/strep. Primary murine lung endothelial cells were cultured in endothelial cell medium growth medium containing 5% FBS, 1.5% endothelial cell growth supplement, and pen/strep (CellBiologics, # M1168). E0771.LMB and E0771.luc cells and not MMTV-Wnt-1, MEFs, or primary cells were tested for the absence of mycoplasma contamination by PCR amplification detection kit (Applied Biological Materials, #G238). Experiments with cell lines were performed for up to 20 passages, primary cells were used for up to 5 passages.

Mice

All animal experiments were conducted according to protocols approved by the Virginia Commonwealth University Institutional Animal Care and Use Committee (IACUC). Breeding pairs of WT and *Sphk2*$^{-/-}$ mice were on a C57BL/6NJ background and obtained from the Jackson Laboratory. The colonies were maintained in the vivarium at VCU. All experiments were performed with littermates from breeding heterozygous mice. Tail snips for genotyping for background strain determination showed that 100% of the genome scan SNP panel tested was matched.

To study tumor progression and lung metastasis, 8–9 weeks old female mice were bilaterally implanted in the 4th mammary fat pads with 20 μL of DMEM (glucose- and phenol red-free, Gibco #A14430–01) containing 0.1×10^6 E0771.LMB murine breast cancer cells expressing mCherry, or MMTV-Wnt1 or E0771.luc murine breast cancer cells. Palpable tumor size was measured using calipers, and the volume was calculated using the formula $V = (W^2\times L)/2$, where V is the tumor volume, W is the tumor width, and L is the tumor length.

In some experiments, E0771.LMB cells were inoculated into the mammary pads, either alone or together, with WT or SphK2 null MEFs in a 1:1 ratio. To determine metastatic pulmonary colonization, 8–9 week old male mice were injected intravenously with 0.5×10^6 E0771.LMB (mCherry+) cells in 100 μL of HBSS (VWR #02-0121-0500). In some experiments, mice were injected i.p. with the SphK2 inhibitor SLM6031434 (2 mg/kg) or the vehicle every other day. Mice were sacrificed by 5% isoflurane inhalation, blood was collected, the mouse perfused as indicated, tissues were removed for analyses, tumors were excised and weighed, fixed in formalin, and embedded in paraffin or frozen in liquid nitrogen.

Treatment of Rag2$^{-/-}$ Il2rg$^{-/-}$ mice with SphK2 inhibitor

Female *Rag2*$^{-/-}$*Il2rg*$^{-/-}$ mice (C57BL/6NTac.Cg-*Rag2*^{tm1Fwa} *Il2rg*^{tm1Wjl}) and C57BL/6NTac control mice were purchased from Taconic Farms. 0.1×10^6 E0771.LMB murine breast cancer cells in 20 μL of DMEM were bilaterally implanted in the 4th mammary fat pad. When tumors reached a palpable size (approximately 20–30 mm^3), usually within 5–7 days or 10–12 days for *Rag2*$^{-/-}$*Il2rg*$^{-/-}$ mice and C57BL/6NTac controls, respectively, the mice received intratumoral injections of SLM6031434 (2 mg/kg) into tumors on the left side and vehicle into tumors on the right side every other day until the humane endpoint. In some experiments, bilateral tumor-bearing C57BL/6NTac mice were injected intraperitoneally with SLM6031434 (2 mg/kg) or vehicle every other day.

Conditioned Medium

Conditioned media (CM) from MEFs or primary fibroblasts was prepared by culturing 0.5×10^6 cells in 6-well plates to confluency in DMEM containing 10% FBS or in fibroblast growth medium containing 2% FBS and 1% fibroblast growth supplement, respectively. The medium was replaced by DMEM or fibroblast medium, both containing 0.5% FBS, without growth supplements. CM was collected 2 d later and filtered through a 0.2 μm filter. In some experiments, MEFs were treated with 10 μM SLM6031434 (gift from Dr. Kevin Lynch) or 10 μM ABC294640 (#10587 Cayman) for 24 h, washed extensively three times to remove the inhibitor, and CM prepared as above. DMEM containing 0.5% FBS or fibroblast medium containing 0.5% FBS incubated in empty wells for 2 days were used as controls.

E0771.LMB Cell Proliferation in Transwell Co-cultures with Fibroblasts

E0771.LMB cells were labeled with 5 μM carboxyfluorescein diacetate succinimidyl ester (CFSE) dye for 5 min in serum-free medium (Invitrogen, CellTrace CFSE). Labeled E0771.LMB cells were cultured in 24-well plates in DMEM containing 10% FBS. MEFs, primary lung fibroblasts, or primary lung endothelial or epithelial cells were plated separately on gelatin-coated 24-well Sarstedt transwell permeable supports (0.4 μm pores) at a density of 50,000 cells/well in DMEM containing 10% FBS, or in fibroblast or epithelial growth medium, respectively. 24 h later, the transwell permeable supports were placed on top of wells with E0771.LMB cells. Plates were incubated for the indicated days, cells in the lower compartments were then detached, fixed in 3.7% paraformaldehyde, and analyzed by flow cytometry with a BD LSRFortessa-X20. The fluorescence values were analyzed by FlowJo software to calculate the proliferation index. Unlabeled and labeled E0771.LMB cells collected at the start of co-culturing were used as controls.

Multicellular Tumor Spheroid Growth and Invasion Assays

Spheroids were cultured according to the manufactureŕs protocol of the Cultrex® 3D Spheroid Fluorometric Proliferation/Viability Assay Kit (Trevigen, Gaithersburg, MD, USA). Briefly, 4,000 E0771.LMB cancer cells in 45 μl cell culture medium per well were mixed with 5 μl cold 10X spheroid formation extracellular matrix (ECM). Next, 50 μl of the single-cell suspension in 1X spheroid formation ECM was added to each well of a 3D culture qualified 96-well spheroid formation plate. The plate was centrifuged at 200 x g for 3 min in a swinging bucket rotor and incubated at 37°C in a tissue culture incubator for 72 h to promote spheroid formation. Then, 50 μl of conditioned media (CM) from primary cells or MEFs was added to each well, and the plate was incubated for 5 days. Spheroid viability was measured by the amount of reduced resazurin with a TECAN Infinite M1000 fluorescence plate reader (Männedorf, Switzerland) with excitation 544 nm and emission 590 nm or the size was visualized microscopically and quantified by image analysis software. The Cultrex® 3D Spheroid BME Cell Invasion Assay Kit (Trevigen) was used for invasion assays. After spheroid formation was established as described above, 50 μl of cell invasion matrix consisting of a basement membrane extract (BME) from the purified from Engelbreth-Holm-Swarm tumor was added to each well. The plate was centrifuged at 200 x g for 3 min in a swinging bucket rotor and incubated at 37°C for 1 h. 100 μl of CM from primary cells or MEFs was added to each well, and the plate was incubated for an additional 5 days. Spheroid invasion was visualized microscopically and quantified by image analysis software.

Quantification and Statistical Analysis

Data are representative of the results obtained from at least three independent experiments to ensure reproducibility. For the *in vivo* lung metastasis and primary tumor growth experiments, the number of mice in each group is indicated in the figure legends. Statistical significance was determined using unpaired two-tailed Student’s t-test with Welchś correction for comparison of two groups unless indicated otherwise, or by ANOVA followed by post hoc tests for multiple comparisons using GraphPad Prism 7.0. For all experiments, the normality of the data from each group was first checked using the Shapiro-Wilk statistical test. For non-normally distributed data, the Mann-Whitney U test was used. Densitometric quantification of immunoblot bands normalized to loading controls was performed using the ImageJ software. The following designations for significance levels are $*p < 0.05$, $**p < 0.01$, and $***p < 0.001$.

Additional materials and methods

Additional materials and methods used in this study can be found in the Supplementary File S1.

Software Availability

RNAseq data generated in this study have been deposited in the NCBI Gene Expression Omnibus with the accession code GSE136655.

Data Availability

All data needed to evaluate the conclusions in the paper are presented in the paper and/or Supplementary Materials.

RESULTS

SphK2 deficiency suppressed tumor growth and lung metastasis, re-programming the tumor microenvironment

High levels of circulating S1P have been linked to increased tumor growth and metastasis (5–7). Unexpectedly, we found that genetic loss of SphK2, which greatly increases circulating levels of S1P in mice (9), markedly decreased, rather than increased, tumor growth in orthotopically implanted E0771.LMB murine TNBC compared to that in wild-type (WT) littermates (Figure 1A,B). Consistent with the profound effects on tumor size in SphK2$^{-/-}$ mice, there was a significant decrease in tumor cell proliferation as determined by Ki-67 staining (Figure 1C). In agreement with previous studies (10), E0771.LMB tumor cells spontaneously metastasized to the lungs of the WT mice. Lung metastatic spread was also greatly reduced in SphK2$^{-/-}$ mice (Figure 1D,E). To validate and broaden our findings, other transplantable syngeneic breast cancer models were used. Growth of mammary tumors from implanted E0771.luc or MMTV-Wnt1 cells were significantly decreased in SphK2$^{-/-}$ mice compared to WT (Supplementary Figure 1A-E), as well as a reduction in lung metastases (Supplementary Figure 1F). In addition, treatment of WT mice bearing E0771.LMB tumors with the potent isozyme-specific SphK2 inhibitor SLM6031434 (11) greatly reduced tumor growth and lung metastases (Supplementary Figure 1G-J).

Tumor progression is not only dictated by the cancer cells themselves, but is also profoundly influenced by interactions between cancer cells and their microenvironment, which includes stromal and immune cells. The tumor microenvironment shapes the immunological landscape and plays a vital role in determining whether the primary tumor is eradicated or metastasizes (3). To assess the involvement of SphK2 in the tumor microenvironment, immune cell infiltration into primary tumors was evaluated by flow cytometry (Supplementary Figure 2A-F). Although there were no differences in the overall frequencies of CD45 positive cells, in the tumor microenvironment lacking SphK2, there were significant increases in the percentages of effector T cells ($CD3^+CD4^+CD44^{hi}CD62L^-$ and $CD3^+CD8^+CD44^{hi}CD62L^-$) and CD4 or CD8 T cells expressing IFN-γ, as well as increased natural killer (NK) cells with high expression of INF-γ, a cytokine that promotes anti-tumor immune responses (Figure 1F). Conversely, immunosuppressive regulatory T cells ($CD3^+CD4^+FoxP3^+CD25^+$) and polymorphonuclear myeloid-derived suppressor cells (PMN-MDSCs, $CD45^+CD11b^+Ly6G^+Ly6C^{lo}$), which represent more than 80% of all MDSCs and play a key role in immune suppression in cancer (12), were significantly decreased in SphK2$^{-/-}$ mice (Figure 1F). Furthermore, SphK2 deletion reprogrammed tumor-associated macrophages (TAMs) towards an M1-like phenotype (Figure 1F). These ‘‘classically activated’’ M1 macrophages, with upregulation of major histocompatibility complex II (MHC-II) and CD86, are capable of cancer cell killing (13). Comparable changes in infiltrating immune cells in the lung microenvironment of tumor-bearing SphK2$^{-/-}$ mice were noted (Supplementary Figure 3), with a decrease in immunosuppressive populations

of regulatory T cells and PMN-MDSCs, increased percentages of CD4 and CD8 T effector cells, and increased NK cells with high expression of INF-γ and M1-like macrophages (Supplementary Figure 3).

The experimental metastasis assay of tail vein injections of E0771.LMB cells that home into the lungs was used to directly examine the effects of deletion of SphK2 in mice on pulmonary colonization. Lung colonization was significantly decreased in SphK2$^{-/-}$ mice compared to that in WT littermates (Figure 2A-C). Similarly, treatment of mice with SLM6031434 to inhibit SphK2 after inoculation of E0771.LMB cells greatly suppressed metastatic colonization, as shown by histological analysis of metastatic lung nodules and QPCR of the mCherry reporter gene present only in the tumor cells (Figure 2D,E).

To distinguish the importance of infiltrating immune cells from other microenvironmental factors, bilateral tumors were generated in the mammary fat pads of *Rag2*$^{-/-}$*Il2rg*$^{-/-}$ mice lacking functional T, B, and NK cells that developed after a shorter latency than their *Rag2*$^{+/+}$*Il2rg*$^{+/+}$ controls. The left tumors of each mouse were injected with SLM6031434, whereas the right tumors received vehicle, allowing meaningful comparisons of the effects of SphK2 inhibition in the same tumor microenvironment (Figure 2F). Notably, SLM6031434 local administration induced marked tumor regression only at the injected site and not on the contralateral tumors in *Rag2*$^{-/-}$*Il2rg*$^{-/-}$ mice as well as in *Rag2*$^{+/+}$*Il2rg*$^{+/+}$ controls (Figure 2F). Moreover, systemic intraperitoneal injections of SLM6031434 inhibited tumor growth to a similar extent as did intratumoral delivery (Figure 2F). Taken together, our results suggest that deletion or inhibition of SphK2 creates a hostile anti-tumor microenvironment that only partially depends on innate and adaptive immune cells.

SphK2, bioactive sphingolipid metabolites, and p53

It was of interest to determine how deletion or inhibition of SphK2 profoundly alters the tumor microenvironment. S1P levels in circulation are increased in SphK2 knockout mice or in mice treated with the SphK2 inhibitor SLM6031434 (9), probably due to reduced clearance by the liver (14). However, in perfused lungs, S1P levels, as expected, decreased with concomitant increases in the levels of its precursor ceramides, particularly C16:0, C20:0, C22:0, and C24:0 species (Figure 3A). Similar tendencies were observed in SphK2$^{-/-}$ mouse embryonic fibroblasts (MEFs) and WT MEFs treated with SLM6031434, with a predominant increase in C16-ceramide (Figure 3B).

We focused our attention on p53 since it was recently shown that C16-ceramide binds p53 and disrupts its interaction with the E3 ubiquitin ligase MDM2, leading to p53 accumulation (15). Second, numerous studies have shown that increased endogenous ceramides can activate p53 (16). Third, strong translocation of p53 to the nucleus was observed in SphK2 null fibroblasts compared to that in WT fibroblasts (Figure 3C,D). To confirm that increased ceramides have the same effect on p53 as SphK2 deletion, WT MEFs were treated with C16-pyridinium ceramide. Consistent with a previous report (15), this water-soluble C16-ceramide analog significantly induced the translocation of p53 to the nucleus (Figure 3D). We also took advantage of the known observation that treating cells with cell-permeable D-erythro-C6-ceramide, but not L-erythro-C6-ceramide, caused a

significant increase in the levels of endogenous long-chain C16:0-ceramide and, to a lesser extent, C24:1-ceramide, because the generation of endogenous ceramides from C6-ceramide via deacylation/reacylation is highly stereospecific (17). Only D-erythro-C6-ceramide, and not L-erythro-C6-ceramide or S1P, induced strong translocation of p53 to the nucleus in WT MEFs compared to vehicle treatment (Figure 3D). Moreover, p53 and phospho-p53 (Ser15), which increases its transcriptional activity (18), were also markedly increased in lungs with pulmonary metastatic nodules from SphK2$^{-/-}$ compared to WT mice (Figure 3E). Importantly, very little p53 staining was observed in the lungs of tumor-bearing WT mice compared to those of SphK2$^{-/-}$ mice (Figure 3F), where the increased staining of p53 was most evident in stromal fibroblasts, but not in the lung epithelium (Figure 3G). Fibroblasts constitute a significant component of tumor stroma and play important roles in tumorigenesis and metastasis (2,19).

Deletion of SphK2 markedly reduces cancer associated fibroblasts signature

As a first step in understanding how SphK2 and p53 act in the microenvironment, we compared the global transcriptomes of WT and SphK2 null MEFs by RNA-seq. The expression profile of SphK2 null fibroblasts differed substantially from that of WT, and at 0.05 False Discovery Rate threshold out of 46,983 tested transcripts, 11,582 genes (5592 upregulated and 5990 downregulated) were differentially expressed (Figure 4A,B and Supplementary Dataset Table 1). As expected, numerous top genes that were previously identified in at least 10 genome-wide datasets as p53-activated targets (20), including CDKN1A, GDF15, GADD45A, TIGAR, and FAS, were upregulated (Figure 4C and Supplementary Dataset Table 2). Gene ontology (GO) and KEGG enrichment analyses of the transcriptional profiles identified potential processes affected by SphK2 deletion (Supplementary Dataset Table 3). The most downregulated genes in SphK2 null cells showed significant enrichment of functional pathways related to extracellular matrix (ECM) organization and degradation, and regulation of cell adhesion and motility (Figure 4D). As previous studies suggested a novel non-cell autonomous function for p53 in normal fibroblasts to suppress their activation to cancer-associated fibroblasts (CAFs), a major contributor in the microenvironment to cancer-associated changes in ECM architecture (21–25), we examined in more detail the effects of SphK2 deletion. The most commonly used genes/markers that identify CAFs, including alpha-smooth muscle actin (αSMA, ACTA2), collagen expression, fibroblast activation protein alpha (FAP), and fibroblast-specific protein 1 (FSP1), also known as S100A4, which regulates both cytoskeletal integrity and cell cycle progression, integrin-alpha 11 (ITGA11), and platelet-derived growth factor receptor (PDGFRα/β), were all markedly reduced by the deletion of SphK2 (Figure 4E), consistent with the decrease in αSMA and type 1 collagen (Col1a1) (Figure 4F). Of the extensive list of 227 CAF-related genes compiled from literature searches (25,26), 150 exhibited a statistically significant coordinate reduction in SphK2 null fibroblasts (Supplementary Dataset Table 4), and a hypergeometric test revealed a highly significant reduction in "CAFness" ($p=1.8^{-11}$). Key ECM-remodeling proteases, matrix metalloproteinases (MMPs) that promote motility and invasion of cancer cells (Figure 4E), and growth factors, including HGF, PDGF, VEGF, FGF, and TGF-β, which are known to be produced and released by CAFs, were downregulated in SphK2 null fibroblasts (Figure 4E). Moreover, CAF-derived cytokines and chemokines that recruit immunosuppressive cells into the tumor

microenvironment to assist in immune evasion (2,19) were significantly reduced (Figure 4E).

Next, we examined the expression of these CAF-associated genes in the lungs, as tumor cells are not the predominant cellular subset in the lung microenvironment. Importantly, deletion of SphK2 greatly reduced the expression of CAF-associated genes in the lungs of mice with breast tumors (Figure 5A) and metastatic nodules (Figure 5B). As expected, deletion of SphK2 also significantly upregulated p53 target genes in tumors (Figure 5C), lungs with metastatic nodules (Figure 5D), and in mice treated with the SphK2 inhibitor (Supplementary Figure 4A,B). Levels of the CAF marker αSMA protein in tumors and lungs with metastases were also markedly reduced by SphK2 deletion (Figure 5E,F). Thus, consistent with p53 stabilization in SphK2 null stromal fibroblasts, gene expression profiling revealed a strongly decreased signature of CAF-related genes, which are key effectors that fuel cancer progression and promote a pro-tumorigenic microenvironment (27,28).

Cancer cells promote resident and recruited normal fibroblasts to acquire the features of CAFs (27,28). In normal breast tissues, smooth muscle cells around the microvasculature are weakly positive for αSMA. However, the activated myofibroblast marker αSMA was highly expressed, particularly in fibroblasts with large spindle cell morphology, which were widely present in the stroma of breast carcinoma from WT mice and nearly absent in SphK2 knockout mice (Figure 5G). Strong αSMA staining in the lungs of WT mice was also observed in the juxtaposition of pulmonary metastatic nodules, but not in SphK2$^{-/-}$ mice (Figure 5H) or in mice treated with the SphK2 inhibitor SLM6031434 (Supplementary Figure 4C). Together, these results indicate that the lack of SphK2 or its inhibition in stromal fibroblasts suppresses the activation of CAFs *in vivo.*

Inhibition of SphK2 suppresses activation of human primary mammary fibroblasts

Previously, it was suggested that cancer cells secrete factors that suppress p53 activity in fibroblasts and reprogram them into pro-tumorigenic CAFs (29). Indeed, we observed enhanced expression of the CAF activation marker αSMA and SphK2 as well as decreased phosphorylation of p53 on Ser15 in human primary mammary fibroblasts when co-cultured with E0771.LMB cells seeded on transwell inserts (Supplementary Figure 5A,B). Moreover, pretreatment of human mammary fibroblasts with the SphK2 inhibitor SLM6031434 increased phosphorylation of p53 and reduced αSMA in this co-culture (Supplementary Figure 5A,B).

Similarly, analysis of *SphK2* expression in the publicly available gene expression database (GSE41678) revealed that co-culturing of two human fibroblast lines (HFFF2 and HFF1, shown to promote tumorigenicity (30)) with MDA-MB-231 triple negative breast cancer cells increased *SphK2* expression in these fibroblasts. In contrast, co-culturing MDA-MB-231 cells with two other human fibroblast lines (Wi-38 and CCD1112Sk that were previously shown not to promote tumorigenesis in vivo (30)), did not increase *SphK2* expression (Supplementary Figure 5C). To assess if upregulation of *SphK2* in CAFs is relevant to human breast cancer, we analyzed publicly available data sets. *SphK2* expression is increased in tumor-associated breast stroma microdissected by laser-capture from 53 patients with invasive ductal carcinoma (31) (Supplementary Figure 6A). Moreover, *SphK2*

was significantly overexpressed in 1097 cases of breast cancer compared with 114 normal samples from TCGA Research Network (https://www.cancer.gov/tcga) (Supplementary Figure 6B). Higher *SphK2* expression also correlated with poor prognosis, particularly with higher grades of breast cancer (Supplementary Figure 6C).

Deletion of SphK2 suppresses the CAF-like secretome in a p53-dependent manner

As mentioned above, CAFs secrete MMPs, growth and angiogenic factors, and cytokines that promote tumor growth, invasion, and metastasis (27). They can also produce cytokines/chemokines that influence the recruitment and function of several types of innate and adaptive immune cells to create a more supportive tumor microenvironment (32). Because previous studies have suggested that in cultured mouse fibroblasts, p53 suppresses the expression of some of these pro-tumorigenic factors (23–25,33), we next examined the involvement of p53 in changes of the CAF-like secretome due to deletion of SphK2. Consistent with the reduction in CAF signature genes (Figure 5A,B), the expression of MMP2, TGF-β, and IL-6, which increased cancer cell proliferation and metastasis and negatively regulated NK and T cell cytotoxic activity (32), was markedly decreased by deletion of SphK2 (Figure 6A). Downregulation of p53 in SphK2 deleted fibroblasts with lentivirus expressing p53-specific shRNA reversed this suppression (Figure 6A). Likewise, expression of the chemokines CCL2, CXCL1, CXCL12, and CSF1, which recruit MDSCs and influence M1 macrophage polarization, and the potent angiogenic factors VEGF-C and CXCL12, as well as CCL5, which also promote recruitment of Tregs (32), were all significantly reduced by SphK2 deletion, effects that were all negated by the downregulation of p53 (Figure 6A). These data suggest that repression of the secretome in SphK2 knockout fibroblasts is mediated by p53. Changes in cytokines and chemokines were confirmed by LEGENDplex multiplex immunoassays (Supplementary Figure 7A). Pretreatment of WT MEFs or primary human mammary fibroblasts with the SphK2 inhibitor also suppressed secretion of these cytokines and chemokines (Supplementary Figure 7A,B). The effect on CXCL12 is particularly interesting, as the CAF secretome is maintained during tumor progression by a CXCL12 autocrine signaling loop (34). Furthermore, it has been shown that CAFs enhance CXCL12–dependent growth of breast cancer cells *in vitro* and in a mouse model (35), and p53 status in stromal fibroblasts modulates tumor growth in a CXCL12-dependent manner (24).

Non-cell autonomous functions of the SphK2/p53 axis in stromal fibroblasts

Numerous growth factors (e.g., IGF, HGF, FGF, PDGF, and SDF1/CXCL12) secreted by CAFs can strongly enhance the growth of the adjacent cancer cells themselves (19), and functional p53 suppresses the production of these tumor-promoting factors (24). To explore the consequences of the curtailed secretome due to the loss of SphK2 and increased p53, we compared the ability of conditioned medium (CM) from WT MEFs or primary lung fibroblasts to induce the growth and survival of E0771.LMB cells with that of CM from SphK2 null fibroblasts. Colony formation of E0771.LMB cells was greatly reduced by adding CM from SphK2 null MEFs compared to that from WT MEFs (Figure 6B). Addition of S1P to the CM from SphK2 null MEFs or downregulation of p53 reduced this suppression (Figure 6B). Similar effects were observed with CM from primary lung fibroblasts isolated from SphK2 knockout mice compared to those from WT lung fibroblasts

or with CM from primary human mammary fibroblasts pretreated with SphK2 inhibitors (Figure 6B). To further confirm this effect, the rate of proliferation of E0771.LMB cells was evaluated by CFSE staining when they were co-cultured with fibroblasts in separate compartments of the transwells (Figure 6C). Indeed, their proliferation was much greater when co-cultured with WT MEFs compared to SphK2 null cells, and downregulation of p53 in SphK2 deleted MEFs reversed this suppression (Figure 6C). Importantly, greater proliferation of these breast cancer cells was also observed when they were co-cultured with primary lung fibroblasts isolated from WT mice compared to those isolated from SphK2 knockout mice (Figure 6C). However, neither primary epithelial cells nor primary endothelial cells from SphK2 knockout mice showed this differential effect on breast cancer cell proliferation compared with their WT counterparts (Figure 6C).

Next, we examined the 3D *in vitro* growth and invasion of multicellular tumor spheroids, which mimic aspects of dimensionality, cell-cell contact, and cell-matrix interactions of *in vivo* solid tumors (36). The growth and viability of E0771.LMB spheroids in 3D culture (Figure 6D and Supplementary Figure 8A) and invasion into the surrounding ECM (Figure 6E and Supplementary Figure 8B) were significantly enhanced only in the presence of CM from primary WT lung fibroblasts, but not from SphK2$^{-/-}$ fibroblasts (Figure 6D,E). Similarly, CM from SphK2$^{-/-}$ MEFs or from WT MEFs as well as from primary human mammary fibroblasts treated with SphK2 inhibitors repressed spheroid growth or invasion into a matrix composed of basement membrane proteins (Figure 6D,E, and Supplementary Figure 8A,B). Once again, knockdown of p53 or addition of S1P reversed the effects of SphK2 deletion or inhibition (Figure 6D,E). Taken together, these results indicate that soluble factors secreted from fibroblasts in an SphK2/p53 axis-dependent manner play a role in enhancing the growth of cancer cells and their invasion.

Loss of SphK2 in fibroblasts suppresses tumor growth

CAFs promote tumor growth and cancer progression (2,19). To examine the effect of SphK2 loss in fibroblasts with a reduction of the CAF-like secretome on tumor progression *in vivo*, we used a syngeneic murine breast cancer model in which E0771.LMB breast cancer cells were co-injected into the mouse mammary fat pad with WT or SphK2 null MEFs. Consistent with previous studies (21,24,37), WT fibroblasts enhanced tumor growth and increased tumor weight (Figure 7A,B). In sharp contrast, SphK2 null fibroblasts did not enhance tumor growth or even decrease tumor weight (Figure 7A,B). Accelerated tumor growth by WT fibroblasts was accompanied by increased proliferation, as determined by Ki-67 staining, whereas SphK2 null MEFs reduced it (Figure 7C,D). The differential effects of WT and SphK2 null fibroblasts on tumor growth depended, at least in part, on p53, as downregulation of p53 in SphK2 null MEFs completely prevented the negative impact of SphK2 null MEFs on tumor growth (Figure 7E,F) and correlated with changes in staining of the CAF marker αSMA (Figure 7G). We speculate that the observed reduction in αSMA staining in the tumor sections from mice inoculated with E0771.LMB together with SphK2 null MEFs compared to those inoculated only with E0771.LMB (Figure 7G) is because SphK2 deletion suppresses their activation to CAFs, which are the cells in the vicinity of the tumors. Alternatively, SphK2 deleted fibroblasts may also reduce the activation of nearby stromal fibroblasts into CAFs due to the reduction in autocrine signaling loops as we found

that in the presence of E0771.LMB cells, co-culturing SphK2$^{-/-}$ MEFs with WT MEFs reduced the overall expression of αSMA (Supplementary Figure 5A).

Finally, E0771.LMB cells were co-injected with WT or SphK2$^{-/-}$ MEFs into the left and right mammary fat pads of *Rag2*$^{-/-}$*Il2rg*$^{-/-}$ mice. Much larger tumors were formed in *Rag2*$^{-/-}$*Il2rg*$^{-/-}$ mice or *Rag2*$^{+/+}$*Il2rg*$^{+/+}$ mice on the side co-injected with WT MEFs compared to those on the opposite side co-injected with SphK2 null MEFs (Figure 7H), supporting the notion that direct CAF-tumor interaction is an important driver of tumor growth, independent of immune cells (38,39). Hence, in agreement with our *in vitro* observations, the reduced expression of secreted pro-tumorigenic factors in SphK2 null stromal fibroblasts resulted in cancer-suppressing effects *in vivo* to restrict tumor growth. Altogether, our work reveals a surprising role for SphK2 in stromal fibroblasts in creating a hospitable tumor microenvironment.

DISCUSSION

Bidirectional communication between cancer cells and their microenvironment influences breast cancer progression, metastasis, therapy resistance, and patient outcome. Targeting components of the tumor microenvironment, such as clinical success with cancer immunotherapy using checkpoint blockade (40), has stimulated great interest in understanding how the microenvironment influences tumor progression with the hope of developing novel therapeutic approaches that activate anti-cancer responses (3).

Here, we report that deletion or inhibition of SphK2 in mice suppressed TNBC progression and lung metastasis caused by reprogramming the tumor microenvironment. We found that the deletion or inhibition of SphK2 decreased S1P and increased ceramides, including C16-ceramide, which increased and activated the tumor suppressor p53 in stromal fibroblasts. In agreement with our studies, treatment of tumor-bearing mice with the SphK2 inhibitor ABC294640 also decreased S1P levels, increased ceramide levels in cells and plasma, and reduced tumor growth (41). Moreover, administration of C6-ceramide induces p53 activation (phosphorylation at Ser15 and increased protein levels) and inhibits xenograft growth (42). Consistent with our preclinical data in mice, a recent study reported that higher levels of ceramides, predominantly C16:0, C22:0, C24:1, and C24:0 species, and reduction in S1P in breast cancer tissue were associated with less aggressive cancer with lower nuclear grade (43). Although ceramide elevation is generally considered a pro-apoptotic event, different ceramide species in specific subcellular compartments have unique functions (4). It has recently been suggested that C16-ceramide is a natural regulatory ligand of p53 that disrupts its complex with the E3 ligase MDM2, leading to p53 stabilization, nuclear translocation, and activation of its downstream targets (15). Consistent with this finding, deletion or inhibition of SphK2 was also accompanied by increased ceramide and transcriptional activity of p53 in MEFs, as well as in interstitial fibroblasts in lungs with metastases.

While most of the p53 research has been primarily focused on its cell-autonomous functions as a tumor suppressor, there is growing evidence for the importance of its non-cell-autonomous functions in the microenvironment (23–25,44–46). Consistent with our work, breast tumors containing p53-deficient fibroblasts developed faster and more

aggressively than those containing wild-type p53 fibroblasts (21). Furthermore, deletion of p53 in resident normal fibroblasts augments their acquisition of a CAF phenotype (25) and promotes the expression of CXCL12 (23,24) which enhances tumor invasion and malignancy. Conversely, stabilization of p53 by small-molecule MDM2 antagonists such as nutlin-3a attenuates the ability of fibroblasts to stimulate breast cancer aggressiveness (46). Indeed, we observed that deletion of SphK2, leading to p53 stabilization in stromal fibroblasts, markedly suppressed their activation to CAFs, which are key players in the crosstalk between tumor cells and their microenvironment (Figure 8). Growth and angiogenic factors produced by CAFs, including CXCL12, TGF-β, IL-6, and VEGF, which directly facilitate tumor growth, and MMPs that initiate remodeling of the extracellular matrix and enhance cancer cell migration and invasion, were all greatly attenuated in the absence of SphK2 in a p53-dependent manner. In addition, cytokines and chemokines produced by CAFs that favor the recruitment and differentiation of MDSCs and Tregs and influence M1 macrophage polarization, as well as immunosuppressive factors such as TGF-β, IL6, CXCL12, and FAS-L, which inhibit the functions of NK cells and $CD8^+$ cytotoxic T cells in the tumor microenvironment (32,47), were also markedly reduced. Therefore, preventing CAF activation by decreasing SphK2 and activating p53 mitigates all these processes, inducing switching to an active anti-tumor microenvironment and reducing tumor progression and metastasis.

Our observations that deletion of SphK2 in stromal fibroblasts results in p53 accumulation and concomitant lower expression of CAF markers shed light on the mechanism by which endogenous SphK2 regulates breast cancer growth, metastasis, and the tumor microenvironment. Importantly, silencing p53 in SphK2-depleted fibroblasts completely rescued CAF-related markers, the pro-tumorigenic secretome, 3D *in vitro* growth, invasion of multicellular breast tumor spheroids, and tumor growth *in vivo*. Thus, we uncovered a novel role of SphK2 in regulating the non-cell autonomous functions of p53 in stromal fibroblasts involved in their activation to CAFs as a mechanism controlling tumor growth and metastasis. It is now recognized that CAFs in breast cancer are heterogeneous, with distinct subsets (48,49). Although most CAFs exert tumor-promoting activities, others have tumor-suppressive functions, and the mechanisms underlying these opposing effects are of great interest (38,39,50,51). Intriguingly, deletion or inhibition of SphK2 in stromal fibroblasts markedly reduced tumor-promoting activity in the tumor microenvironment without increasing tumor-suppressive functions.

Our data from *in vitro* co-cultures, 3D multicellular tumor spheroids, and co-injection of $SphK2^{-/-}$ MEFs with E0771.LMB breast cancer cells into $Rag2^{-/-}Il2rg^{-/-}$ mice lacking functional T, B, and NK cells, as well as the activity of an SphK2 inhibitor in these immunodeficient mice, suggest that suppression of tumor growth and invasion by deletion or inhibition of SphK2 may only be partially dependent on innate and adaptive immune cells. Rather, our data suggest that direct fibroblast-tumor interactions are the predominant drivers of tumor growth and are regulated by non-cell-autonomous functions of the SphK2/p53 axis in stromal fibroblasts. Nevertheless, we cannot exclude the possibility that CAFs may exert some effects on metastatic growth by regulating anti-tumor immunity, in addition to direct interactions with cancer cells. While there has been a focus in the field of CAF-immune cell interactions (reviewed in (47)), our data are consistent with several recent studies

demonstrating that CAFs promote tumor growth through direct interactions with and effects on the cancer cells themselves, independent of anti-tumor immunity (29,38,39). In this regard, it has been reported that depletion of all CAFs decreases tumor growth and mortality in desmoplastic colorectal and pancreatic metastasis mouse models. However, there had only minor effects on the composition of immune cells in the liver, except for a decrease in Tregs (38). Moreover, in agreement with our results, ablation of p53 in fibroblasts induced their activation to CAFs and enabled them to efficiently promote prostate and skin tumor growth and squamous carcinogenesis in immunodeficient NOD/SCID mice (24,25,29). Consistent with these studies and our data, downregulation of p53 in hTERT-immortalized normal fibroblasts enhanced the growth of H460 lung tumors in SCID mice. However, hTERT-immortalized CAFs derived from the same lung cancer patient reduced the growth of H460 lung tumors, suggesting that p53 in CAFs may have the opposite effect on its role in normal fibroblasts (37).

Nonetheless, the effect of SphK2 in the microenvironment is independent of the p53 status of the cancer cells themselves as deletion of SphK2 in mice greatly reduced tumor growth of implanted E0771.LMB breast cancer cells that express mutant p53 as well as MMTV-Wnt1 breast cancer cells expressing WT p53. Altogether, our data suggest that repression of the CAF-related secretome explains the strong suppression of tumor progression and metastasis in SphK2$^{-/-}$ mice or by the administration of a potent SphK2 inhibitor.

Previous studies have shown that SphK2 inhibitors reduce cancer cell growth and suppress tumor growth in pre-clinical animal models (52,53). Clinical trials with one inhibitor of SphK2, ABC294640, are in progress (NCT02939807, NCT02229981, and NCT02757326). Our data with a more potent and specific SphK2 inhibitor indicate that inhibiting SphK2 is not only cytotoxic to the tumor itself but also prevents the activation of stromal fibroblasts to CAFs, creating an anti-tumor microenvironment for eradicating cancer cells. Thus, SphK2 inhibitors could be considered as a multi-pronged treatment modality to bolster clinical effectiveness.

Since CAFs do not harbor p53 mutations (54), CAF-directed therapy to reprogram them back to their normal resting phenotype is beginning to attract attention. However, identifying such an agent remains elusive (50). Our work suggests that the inhibition of SphK2 and p53 activation in stromal fibroblasts is a component of a mechanism restraining their activation to CAFs and driving tumor regression. Consistent with our findings, local p53 activation in the tumor microenvironment by nutlin-3a led to tumor regression and eradication (55). There already is proof of concept of the potential value of engaging stromal p53 in an anti-cancer response with the development of MDM2/X inhibitors including nutlin-3 now in clinical trials (NCT03654716, NCT03217266, NCT03654716, NCT01877382, NCT03217266) (56). However, only some of these clinical trials stratified patients according to p53 status, and systemic delivery revealed hematological toxicity that is detrimental to immunotherapy (57). Our work suggests a new and different approach to harness the p53 network, which might pave the way for the development of a novel class of therapeutics targeting SphK2 and the microenvironment that interferes with breast cancer progression and metastasis.

Supplementary Material

Refer to Web version on PubMed Central for supplementary material.

Acknowledgments

We are grateful to Dr. Webster Santos (Virginia Tech) and Dr. Kevin Lynch for their generous gift of SLM6031434. We thank Dr. Paula Bos for her helpful advice. We also thank Bin Hu, Julie Farnsworth, and Jeremy Allegood from the core facilities for their skillful technical assistance. This work was supported by the National Institutes of Health under Grant R01GM043880 (S.S.). M.A.M. was supported by the Ruth L. Kirschstein Individual Predoctoral National Service Award (F31 CA220798). S.S. was also supported by DoD W81XWH2010434. The authors acknowledge the Virginia Commonwealth University Lipidomics/Metabolomics, Cancer Mouse Models, Flow Cytometry, and Microscopy Shared Resources, which are supported in part by funding from the NIH-NCI Cancer Center Support Grant P30 CA016059.

References

1. Yates LR, Knappskog S, Wedge D, Farmery JHR, Gonzalez S, Martincorena I, et al. Genomic Evolution of Breast Cancer Metastasis and Relapse. Cancer Cell 2017;32:169–84 e7 [PubMed: 28810143]
2. Hanahan D, Coussens LM. Accessories to the crime: functions of cells recruited to the tumor microenvironment. Cancer Cell 2012;21:309–22 [PubMed: 22439926]
3. Quail DF, Joyce JA. Microenvironmental regulation of tumor progression and metastasis. Nat Med 2013;19:1423–37 [PubMed: 24202395]
4. Ogretmen B. Sphingolipid metabolism in cancer signalling and therapy. Nat Rev Cancer 2018;18:33–50 [PubMed: 29147025]
5. Nagahashi M, Ramachandran S, Kim EY, Allegood JC, Rashid OM, Yamada A, et al. Sphingosine-1-phosphate produced by sphingosine kinase 1 promotes breast cancer progression by stimulating angiogenesis and lymphangiogenesis. Cancer Res 2012;72:726–35 [PubMed: 22298596]
6. Nagahashi M, Yamada A, Katsuta E, Aoyagi T, Huang WC, Terracina KP, et al. Targeting the SphK1/S1P/S1PR1 Axis That Links Obesity, Chronic Inflammation, and Breast Cancer Metastasis. Cancer Res 2018;78:1713–25 [PubMed: 29351902]
7. Ponnusamy S, Selvam SP, Mehrotra S, Kawamori T, Snider AJ, Obeid LM, et al. Communication between host organism and cancer cells is transduced by systemic sphingosine kinase 1/sphingosine 1-phosphate signalling to regulate tumour metastasis. EMBO Mol Med 2012;4:761–75 [PubMed: 22707406]
8. Clark NM, Martinez LM, Murdock S, deLigio JT, Olex AL, Effi C, et al. Regulatory T Cells Support Breast Cancer Progression by Opposing IFN-gamma-Dependent Functional Reprogramming of Myeloid Cells. Cell Rep 2020;33:108482 [PubMed: 33296659]
9. Kharel Y, Raje M, Gao M, Gellett AM, Tomsig JL, Lynch KR, et al. Sphingosine kinase type 2 inhibition elevates circulating sphingosine 1-phosphate. Biochem J 2012;447:149–57 [PubMed: 22747486]
10. Johnstone CN, Smith YE, Cao Y, Burrows AD, Cross RS, Ling X, et al. Functional and molecular characterisation of EO771.LMB tumours, a new C57BL/6-mouse-derived model of spontaneously metastatic mammary cancer. Dis Model Mech 2015;8:237–51 [PubMed: 25633981]
11. Kharel Y, Morris EA, Congdon MD, Thorpe SB, Tomsig JL, Santos WL, et al. Sphingosine Kinase 2 Inhibition and Blood Sphingosine 1-Phosphate Levels. J Pharmacol Exp Ther 2015;355:23–31 [PubMed: 26243740]
12. Gabrilovich DI. Myeloid-Derived Suppressor Cells. Cancer Immunol Res 2017;5:3–8 [PubMed: 28052991]
13. Mantovani A, Marchesi F, Malesci A, Laghi L, Allavena P. Tumour-associated macrophages as treatment targets in oncology. Nat Rev Clin Oncol 2017;14:399–416 [PubMed: 28117416]
14. Kharel Y, Huang T, Salamon A, Harris TE, Santos WL, Lynch KR. Mechanism of sphingosine 1-phosphate clearance from blood. Biochem J 2020;477:925–35 [PubMed: 32065229]

15. Fekry B, Jeffries KA, Esmaeilniakooshkghazi A, Szulc ZM, Knagge KJ, Kirchner DR, et al. C16-ceramide is a natural regulatory ligand of p53 in cellular stress response. Nat Commun 2018;9:4149 [PubMed: 30297838]
16. Jeffries KA, Krupenko NI. Ceramide Signaling and p53 Pathways. Adv Cancer Res 2018;140:191–215 [PubMed: 30060809]
17. Ogretmen B, Pettus BJ, Rossi MJ, Wood R, Usta J, Szulc Z, et al. Biochemical mechanisms of the generation of endogenous long chain ceramide in response to exogenous short chain ceramide in the A549 human lung adenocarcinoma cell line. Role for endogenous ceramide in mediating the action of exogenous ceramide. J Biol Chem 2002;277:12960–9 [PubMed: 11815611]
18. Meek DW, Anderson CW. Posttranslational modification of p53: cooperative integrators of function. Cold Spring Harb Perspect Biol 2009;1:a000950 [PubMed: 20457558]
19. Kalluri R. The biology and function of fibroblasts in cancer. Nat Rev Cancer 2016;16:582–98 [PubMed: 27550820]
20. Fischer M. Census and evaluation of p53 target genes. Oncogene 2017;36:3943–56 [PubMed: 28288132]
21. Kiaris H, Chatzistamou I, Trimis G, Frangou-Plemmenou M, Pafiti-Kondi A, Kalofoutis A. Evidence for nonautonomous effect of p53 tumor suppressor in carcinogenesis. Cancer Res 2005;65:1627–30 [PubMed: 15753354]
22. Hill R, Song Y, Cardiff RD, Van Dyke T. Selective evolution of stromal mesenchyme with p53 loss in response to epithelial tumorigenesis. Cell 2005;123:1001–11 [PubMed: 16360031]
23. Moskovits N, Kalinkovich A, Bar J, Lapidot T, Oren M. p53 Attenuates cancer cell migration and invasion through repression of SDF-1/CXCL12 expression in stromal fibroblasts. Cancer Res 2006;66:10671–6 [PubMed: 17108103]
24. Addadi Y, Moskovits N, Granot D, Lozano G, Carmi Y, Apte RN, et al. p53 status in stromal fibroblasts modulates tumor growth in an SDF1-dependent manner. Cancer Res 2010;70:9650–8 [PubMed: 20952507]
25. Procopio MG, Laszlo C, Al Labban D, Kim DE, Bordignon P, Jo SH, et al. Combined CSL and p53 downregulation promotes cancer-associated fibroblast activation. Nat Cell Biol 2015;17:1193–204 [PubMed: 26302407]
26. Bartoschek M, Oskolkov N, Bocci M, Lovrot J, Larsson C, Sommarin M, et al. Spatially and functionally distinct subclasses of breast cancer-associated fibroblasts revealed by single cell RNA sequencing. Nat Commun 2018;9:5150 [PubMed: 30514914]
27. Chen X, Song E. Turning foes to friends: targeting cancer-associated fibroblasts. Nat Rev Drug Discov 2019;18:99–115 [PubMed: 30470818]
28. Fane M, Weeraratna AT. How the ageing microenvironment influences tumour progression. Nat Rev Cancer 2020;20:89–106 [PubMed: 31836838]
29. Cangkrama M, Wietecha M, Mathis N, Okumura R, Ferrarese L, Al-Nuaimi D, et al. A paracrine activin A-mDia2 axis promotes squamous carcinogenesis via fibroblast reprogramming. EMBO Mol Med 2020;12:e11466 [PubMed: 32150356]
30. Rajaram M, Li J, Egeblad M, Powers RS. System-wide analysis reveals a complex network of tumor-fibroblast interactions involved in tumorigenicity. PLoS Genet 2013;9:e1003789 [PubMed: 24068959]
31. Finak G, Bertos N, Pepin F, Sadekova S, Souleimanova M, Zhao H, et al. Stromal gene expression predicts clinical outcome in breast cancer. Nat Med 2008;14:518–27 [PubMed: 18438415]
32. Ziani L, Chouaib S, Thiery J. Alteration of the Antitumor Immune Response by Cancer-Associated Fibroblasts. Front Immunol 2018;9:414 [PubMed: 29545811]
33. Schmid JO, Dong M, Haubeiss S, Friedel G, Bode S, Grabner A, et al. Cancer cells cue the p53 response of cancer-associated fibroblasts to cisplatin. Cancer Res 2012;72:5824–32 [PubMed: 22962266]
34. Kojima Y, Acar A, Eaton EN, Mellody KT, Scheel C, Ben-Porath I, et al. Autocrine TGF-beta and stromal cell-derived factor-1 (SDF-1) signaling drives the evolution of tumor-promoting mammary stromal myofibroblasts. Proc Natl Acad Sci U S A 2010;107:20009–14 [PubMed: 21041659]

35. Allinen M, Beroukhim R, Cai L, Brennan C, Lahti-Domenici J, Huang H, et al. Molecular characterization of the tumor microenvironment in breast cancer. Cancer Cell 2004;6:17–32 [PubMed: 15261139]
36. Bowers HJ, Fannin EE, Thomas A, Weis JA. Characterization of multicellular breast tumor spheroids using image data-driven biophysical mathematical modeling. Sci Rep 2020;10:11583 [PubMed: 32665565]
37. Arandkar S, Furth N, Elisha Y, Nataraj NB, van der Kuip H, Yarden Y, et al. Altered p53 functionality in cancer-associated fibroblasts contributes to their cancer-supporting features. Proc Natl Acad Sci U S A 2018;115:6410–5 [PubMed: 29866855]
38. Bhattacharjee S, Hamberger F, Ravichandra A, Miller M, Nair A, Affo S, et al. Tumor restriction by type I collagen opposes tumor-promoting effects of cancer-associated fibroblasts. J Clin Invest 2021;131
39. Jungwirth U, van Weverwijk A, Evans RJ, Jenkins L, Vicente D, Alexander J, et al. Impairment of a distinct cancer-associated fibroblast population limits tumour growth and metastasis. Nat Commun 2021;12:3516 [PubMed: 34112782]
40. Ribas A, Wolchok JD. Cancer immunotherapy using checkpoint blockade. Science 2018;359:1350–5 [PubMed: 29567705]
41. Venant H, Rahmaniyan M, Jones EE, Lu P, Lilly MB, Garrett-Mayer E, et al. The Sphingosine Kinase 2 Inhibitor ABC294640 Reduces the Growth of Prostate Cancer Cells and Results in Accumulation of Dihydroceramides In Vitro and In Vivo. Mol Cancer Ther 2015;14:2744–52 [PubMed: 26494858]
42. Chen MB, Jiang Q, Liu YY, Zhang Y, He BS, Wei MX, et al. C6 ceramide dramatically increases vincristine sensitivity both in vivo and in vitro, involving AMP-activated protein kinase-p53 signaling. Carcinogenesis 2015;36:1061–70 [PubMed: 26116623]
43. Moro K, Kawaguchi T, Tsuchida J, Gabriel E, Qi Q, Yan L, et al. Ceramide species are elevated in human breast cancer and are associated with less aggressiveness. Oncotarget 2018;9:19874–90 [PubMed: 29731990]
44. Lujambio A, Akkari L, Simon J, Grace D, Tschaharganeh DF, Bolden JE, et al. Non-cell-autonomous tumor suppression by p53. Cell 2013;153:449–60 [PubMed: 23562644]
45. He XY, Xiang C, Zhang CX, Xie YY, Chen L, Zhang GX, et al. p53 in the Myeloid Lineage Modulates an Inflammatory Microenvironment Limiting Initiation and Invasion of Intestinal Tumors. Cell Rep 2015;13:888–97 [PubMed: 26565902]
46. Wiley CD, Schaum N, Alimirah F, Lopez-Dominguez JA, Orjalo AV, Scott G, et al. Small-molecule MDM2 antagonists attenuate the senescence-associated secretory phenotype. Sci Rep 2018;8:2410 [PubMed: 29402901]
47. Monteran L, Erez N. The Dark Side of Fibroblasts: Cancer-Associated Fibroblasts as Mediators of Immunosuppression in the Tumor Microenvironment. Front Immunol 2019;10:1835 [PubMed: 31428105]
48. Costa A, Kieffer Y, Scholer-Dahirel A, Pelon F, Bourachot B, Cardon M, et al. Fibroblast Heterogeneity and Immunosuppressive Environment in Human Breast Cancer. Cancer Cell 2018;33:463–79 e10 [PubMed: 29455927]
49. Kieffer Y, Hocine HR, Gentric G, Pelon F, Bernard C, Bourachot B, et al. Single-Cell Analysis Reveals Fibroblast Clusters Linked to Immunotherapy Resistance in Cancer. Cancer Discov 2020;10:1330–51 [PubMed: 32434947]
50. Sahai E, Astsaturov I, Cukierman E, DeNardo DG, Egeblad M, Evans RM, et al. A framework for advancing our understanding of cancer-associated fibroblasts. Nat Rev Cancer 2020;20:174–86 [PubMed: 31980749]
51. Chen Y, Kim J, Yang S, Wang H, Wu CJ, Sugimoto H, et al. Type I collagen deletion in alphaSMA(+) myofibroblasts augments immune suppression and accelerates progression of pancreatic cancer. Cancer Cell 2021;39:548–65 e6 [PubMed: 33667385]
52. French KJ, Zhuang Y, Maines LW, Gao P, Wang W, Beljanski V, et al. Pharmacology and antitumor activity of ABC294640, a selective inhibitor of sphingosine kinase-2. J Pharmacol Exp Ther 2010;333:129–39 [PubMed: 20061445]

53. Venkata JK, An N, Stuart R, Costa LJ, Cai H, Coker W, et al. Inhibition of sphingosine kinase 2 downregulates the expression of c-Myc and Mcl-1 and induces apoptosis in multiple myeloma. Blood 2014;124:1915–25 [PubMed: 25122609]

54. Hosein AN, Wu M, Arcand SL, Lavallee S, Hebert J, Tonin PN, et al. Breast carcinoma-associated fibroblasts rarely contain p53 mutations or chromosomal aberrations. Cancer Res 2010;70:5770–7 [PubMed: 20570891]

55. Guo G, Yu M, Xiao W, Celis E, Cui Y. Local Activation of p53 in the Tumor Microenvironment Overcomes Immune Suppression and Enhances Antitumor Immunity. Cancer Res 2017;77:2292–305 [PubMed: 28280037]

56. Tisato V, Voltan R, Gonelli A, Secchiero P, Zauli G. MDM2/X inhibitors under clinical evaluation: perspectives for the management of hematological malignancies and pediatric cancer. J Hematol Oncol 2017;10:133 [PubMed: 28673313]

57. Kastenhuber ER, Lowe SW. Putting p53 in Context. Cell 2017;170:1062–78 [PubMed: 28886379]

Significance:

Sphingosine kinase 2 facilitates the activation of stromal fibroblasts to tumor-promoting cancer-associated fibroblasts by suppressing host p53 activity, revealing sphingosine kinase 2 as a potential target to reprogram the tumor microenvironment.

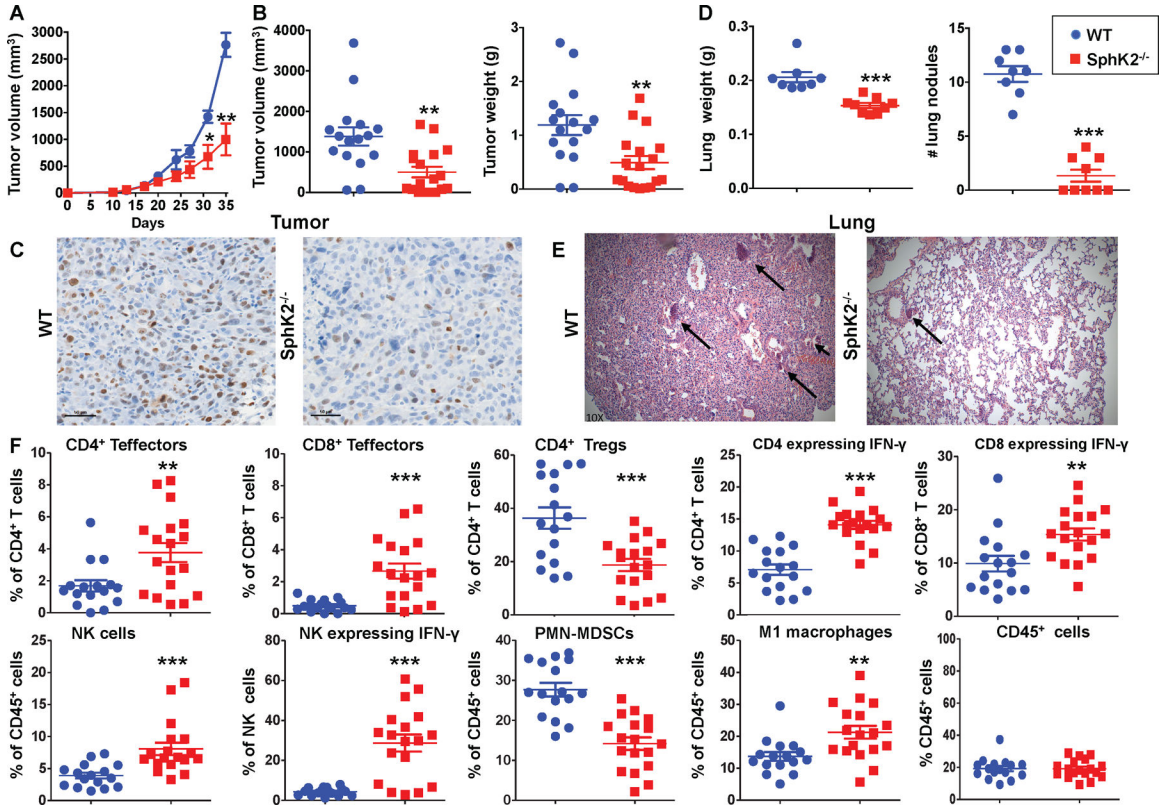

Figure 1. Deletion of SphK2 reduced growth and lung metastasis of syngeneic breast tumors and decreased immunosuppressive microenvironment.

(A-E) Murine E0771.LMB-mCherry breast cancer cells were implanted bilaterally in the mammary fat pads of female WT and SphK2$^{-/-}$ mice. (n=8–9 mice/group, 2 independent experiments). (A) Total tumor volumes were monitored every 5 days. (B-F) Mice were sacrificed at day 35. (B) Individual tumor volumes and weights. (C) Tumor sections were stained with Ki-67 antibody. Proliferation determined by numbers of Ki-67 stained cells per high magnification field was 112 ± 34 and 24 ± 12 for WT and SphK2$^{-/-}$, respectively. (n=6 different fields). Scale bar: 50 μm. (D) Lung metastasis determined by lung weight and quantitation of visible metastatic nodules. (E) Lung sections were stained with H&E (black arrows indicate tumor nodules). (F) Dissociated cells from tumor tissues were stained with fluorochrome-conjugated anti-mouse antibodies and analyzed by multicolor flow cytometry for CD8 Teffectors (CD45$^+$CD3$^+$CD8$^+$CD44$^+$CD62L$^-$), CD4 Teffectors (CD45$^+$CD3$^+$CD4$^+$CD44$^+$CD62L$^-$), CD4 Tregs (CD45$^+$CD4$^+$FoxP3$^+$CD25$^+$), CD4 or CD8 T cells expressing IFN-γ, NK cells (CD45$^+$CD3$^-$NK1.1$^+$) and IFN-γ expressing NK cells (CD45$^+$CD3$^-$ NK1.1$^+$IFN-γ$^+$), PMN-MDSCs (CD45$^+$CD11b$^+$Ly6G$^+$Ly6C^{lo}), M1-like macrophages (CD45$^+$CD11b$^+$F4/80$^+$CD86$^+$MHCII^{hi}), and CD45$^+$ cells (expressed as % of single cells). Data are from 2 independent experiments and are mean ± SEM; *p < 0.05, **p < 0.01, ***p < 0.001. Welch's t-test.

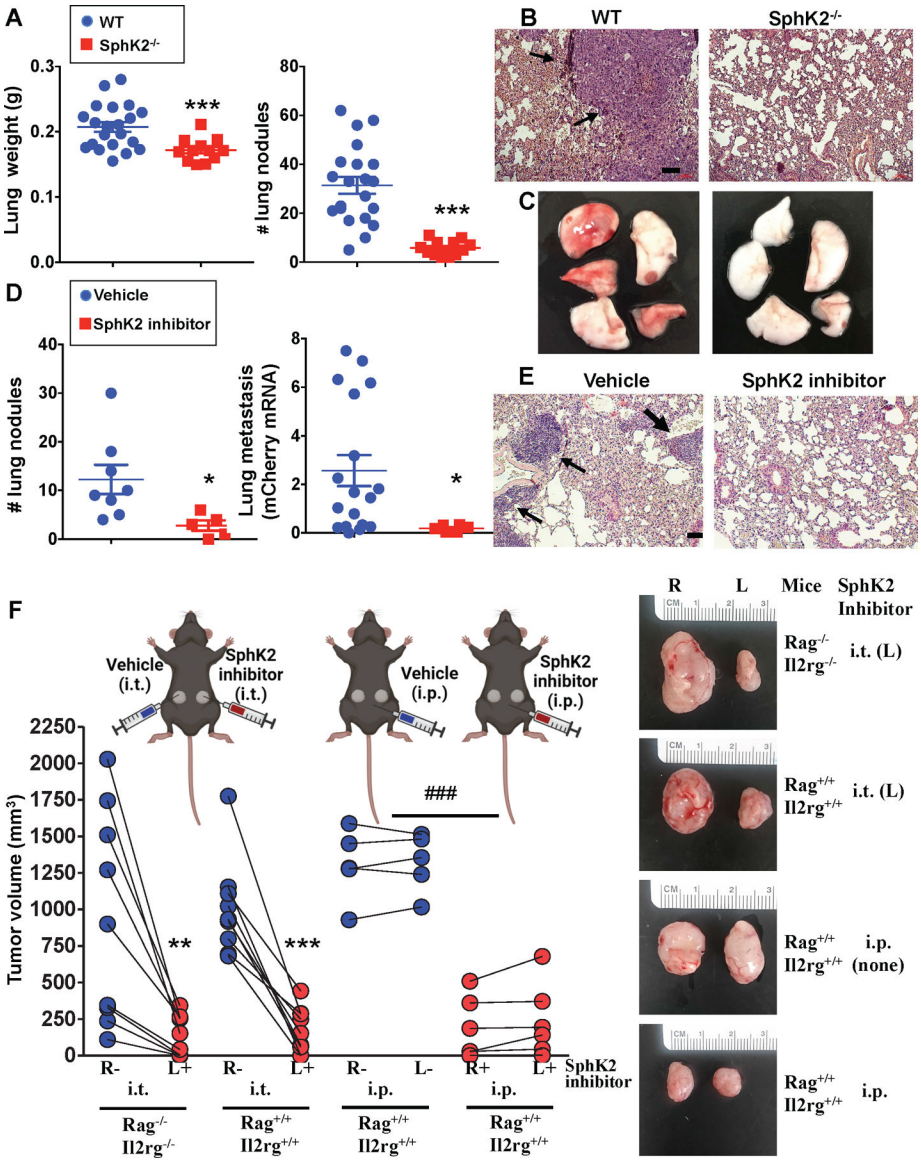

Figure 2. Deletion or inhibition of SphK2 reduces metastatic lung colonization, and SphK2 inhibition induces tumor regression in Rag2$^{-/-}$Il2rg$^{-/-}$ mice.

(A-C) WT and SphK2$^{-/-}$ male mice were intravenously injected with E0771.LMB-mCherry breast cancer cells (n=21 and 12 mice/group, 3 independent experiments). (D,E) WT male mice were intravenously injected with E0771.LMB-mCherry cells and treated 3 d later with SphK2 inhibitor SLM6031434 (2 mg/kg) or vehicle i.p. every other day (n=8 and 5 mice/group). (A,D) Lung metastasis was determined by lung weights, lung nodules, or by quantification of mCherry RNA levels by QPCR normalized to *Gapdh*. (B,E) Lung sections stained with H&E. Arrows indicate tumor nodules. Scale bar: 100 μm. (C) Lung images showing examples of nodules in WT and their absence in lungs from SphK2$^{-/-}$ mice. (F) E0771.LMB cells were implanted bilaterally into the mammary fat pads of female *Rag2*$^{-/-}$*Il2rg*$^{-/-}$ and *Rag2*$^{+/+}$*Il2rg*$^{+/+}$ mice. When palpable tumors reached sizes of 20–30 mm^3, the left tumors (L) were injected intratumorally (i.t.) with SLM6031434 while the right tumors (R) received vehicle every other day. Where indicated, bilateral

tumor bearing *Rag2*$^{+/+}$*Il2rg*$^{+/+}$ mice were treated intraperitoneally (i.p.) with SLM6031434 or vehicle. (n=9,9,5 and 7 mice/group). Schematic of experimental design is shown. Tumor sizes on the sides of SphK2 inhibitor treatment and contralateral sides were measured, and representative images of tumors are shown. (A,C,D) Data are mean ± SEM from 3 independent experiments. Welch's t-test, * $p < 0.05$, ** $p < 0.01$, *** $p < 0.001$. (F) Unpaired two-tailed t-test, ** $p < 0.01$, *** $p < 0.001$ comparing left and right tumors, Welch's t-test, $^{###}p < 0.001$ comparing vehicle i.p. with SphK2 inhibitor i.p.

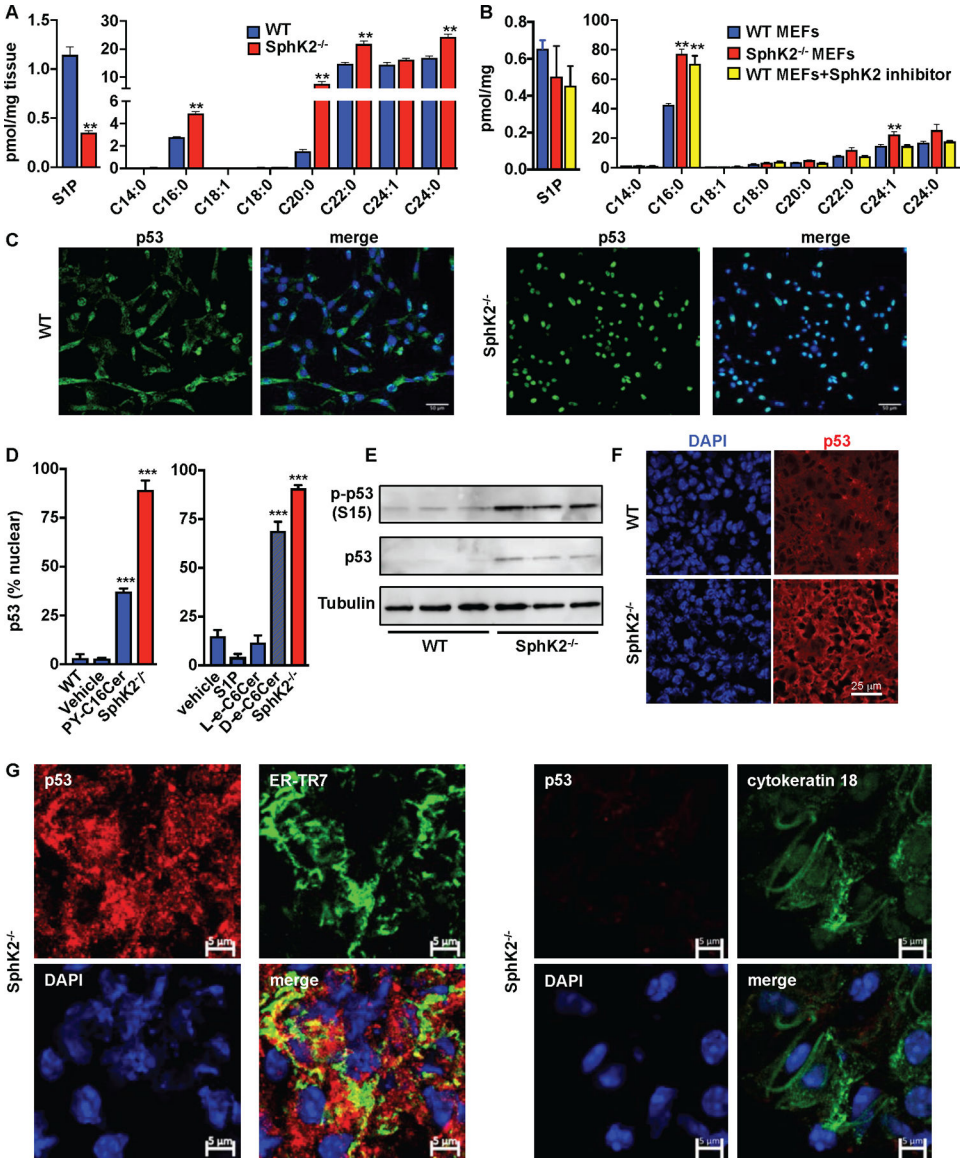

Figure 3. SphK2 deletion increases C16-ceramide and activates p53 in vivo and in vitro.

(A,B) Sphingolipids were determined by LC-ESI-MS/MS in lungs from WT and SphK2$^{-/-}$ mice (A) and in MEFs from SphK2 null and in WT treated without or with 10 μM SLM6031434 for 24 h (B). (n=3). Data are mean ± SD. **p < 0.01 compared to WT. (A) Welch's t-test, (B) One-way analysis of variance test followed by Dunnett's multiple comparisons test. Data are representative of 3 independent experiments. (C,D) SphK2 null or WT MEFs treated for 24 h with vehicle, pyridinium-C16-ceramide (PY-C16Cer, 5 μM), D-erythro-C6-ceramide (D-e-C6Cer, 20 μM), L-erythro-C6-ceramide (L-e-C6Cer, 20 μM), or S1P (100 nM), as indicated, were immunostained for p53. (C) Representative confocal images (green p53; blue, DAPI/nuclei; scale bar: 50 μm) (D) Quantification of nuclear translocation of p53. (n=3,4). Data are mean ± SD. ***p < 0.001 compared to WT or Vehicle. One-way analysis of variance test followed by Dunnett's multiple comparisons test. (E) Lysates of lungs from WT and SphK2$^{-/-}$ mice bearing E0771.LMB mammary tumors on

day 35 after implantation were analyzed by immunoblotting with the indicated antibodies. (n=3). (F,G) Confocal images of lung sections from breast tumor bearing WT and SphK2$^{-/-}$ mice stained for p53 (red) (F), scale bar, 25 μm, and (G) co-stained for ER-TR7 fibroblast-specific marker (green) or for cytokeratin 18 epithelial cell marker (green). Nuclei stained with DAPI (blue). Scale bar: 5 μm.

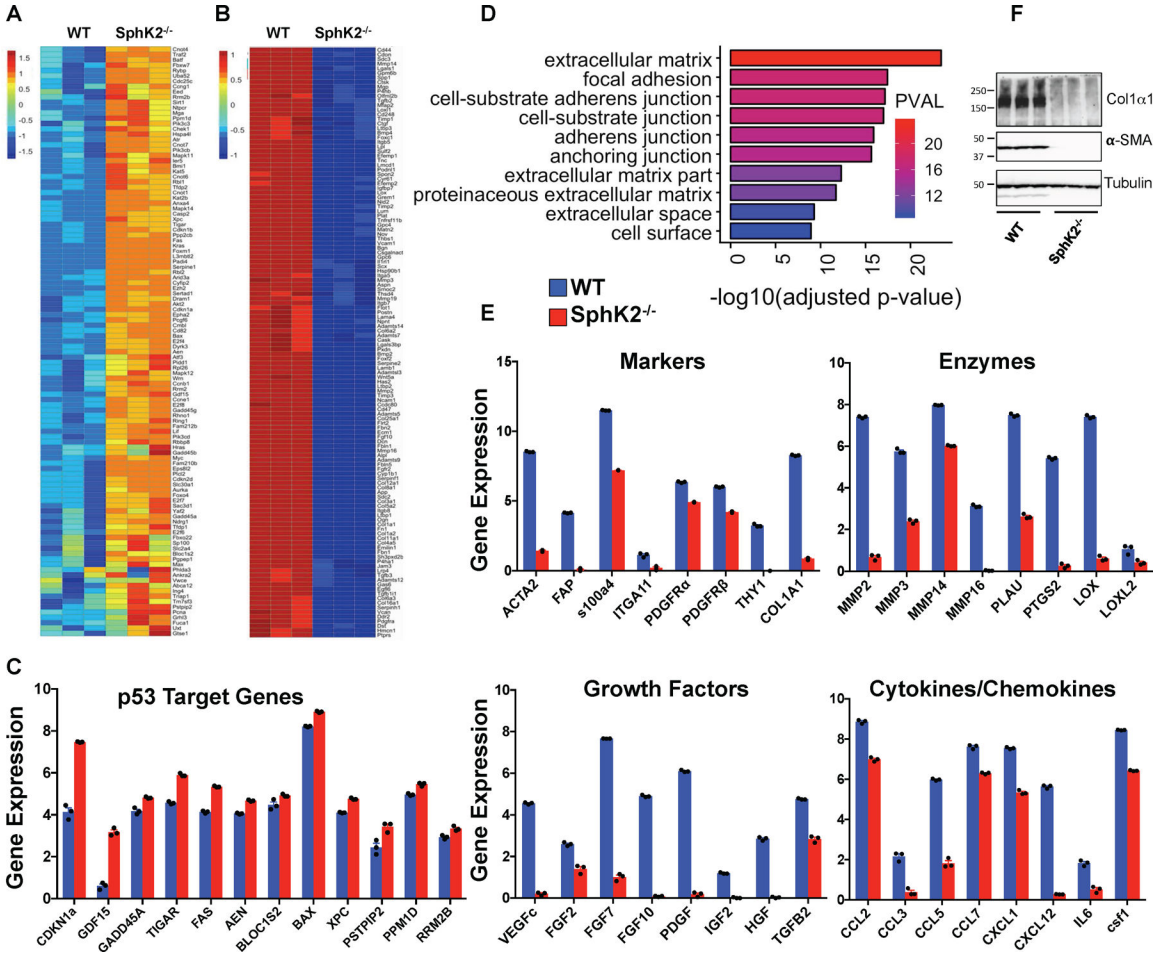

Figure 4. Deletion of SphK2 in fibroblasts suppresses cancer associated fibroblast phenotype.

(A) Heatmap expression matrix of p53 target genes, extracted from the set of genes upregulated in the SphK2 null MEFs. (B) Heatmap expression matrix of the 130 most downregulated genes in SphK2 null fibroblasts. (A,B) Row-scaled log2-transformed transcripts per kilobase million (TPM) values are shown. (C) Expression of selected p53 target genes upregulated in SphK2 null fibroblasts. (D) Gene ontology (GO) enrichment analysis for top biological processes preferentially downregulated by deletion of SphK2. (E) Expression of selected genes, including CAF markers, ECM remodeling enzymes, growth factors, and cytokines/chemokines that are downregulated in SphK2 null fibroblasts. (C,E) Mean ± SD of log2-transformed TPM values are shown. *$p < 0.05$ for all genes shown. (F) WT and SphK2 null fibroblasts were analyzed by immunoblotting.

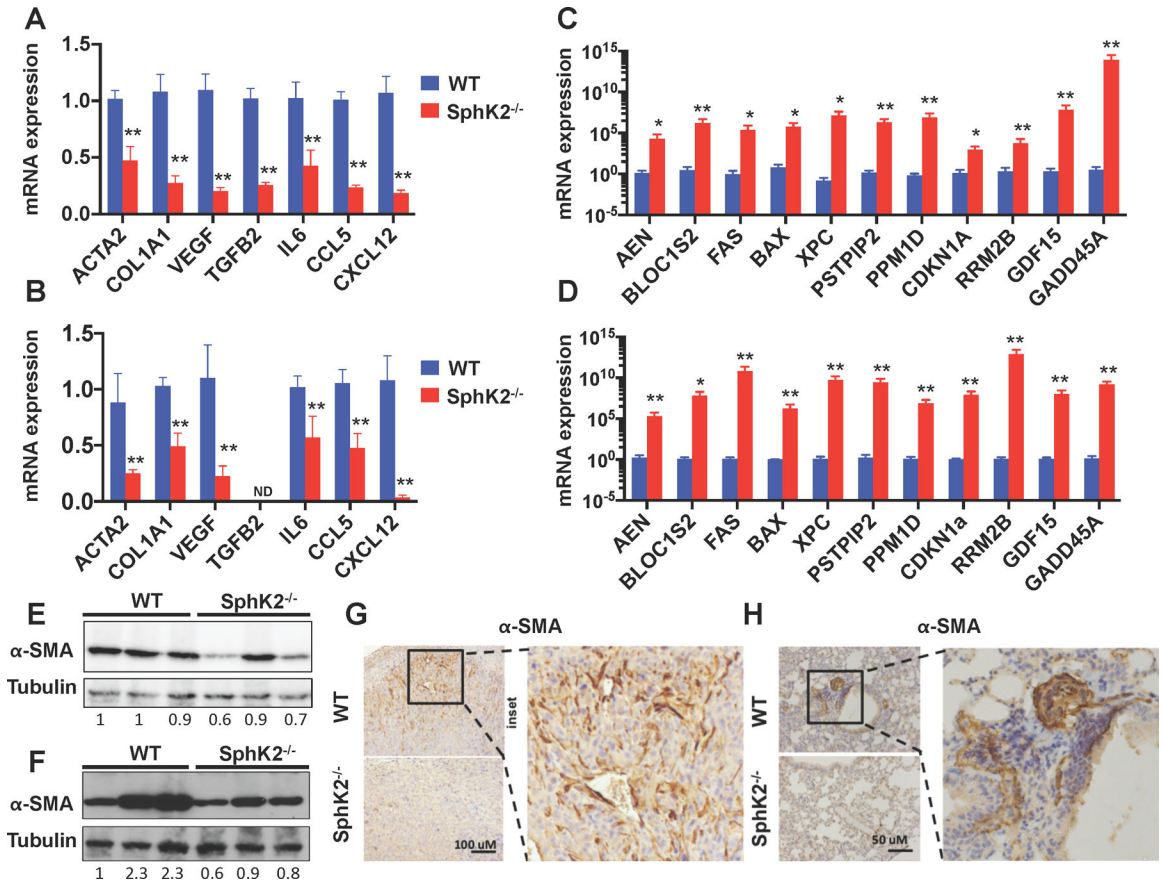

Figure 5. Cancer associated fibroblast features of SphK2 null mice are reduced in mammary tumors and metastatic lung nodules.

(A,B) Expression of CAF signature genes determined by QPCR in lungs from WT and SphK2$^{-/-}$ mice bearing E0771.LMB breast tumors (A) or from mice with pulmonary metastatic nodules (B). (C,D) Expression of specific p53 target genes determined by QPCR in the tumors (C) and in lungs with metastatic nodules (D) (n=4,6). (A,B) *p < 0.05, **p < 0.01 Welch's t-test. (C,D), *p < 0.05, **p < 0.01 two-tailed Mann-Whitney U-test. nd, not detected. (E-H) αSMA determined by immunoblotting and relative densities of the immunopositive bands normalized to Tubulin were quantified (E,F), and by immunohistochemistry (G,H) of breast tumors (E,G) or of lungs with pulmonary metastatic nodules (F,H).

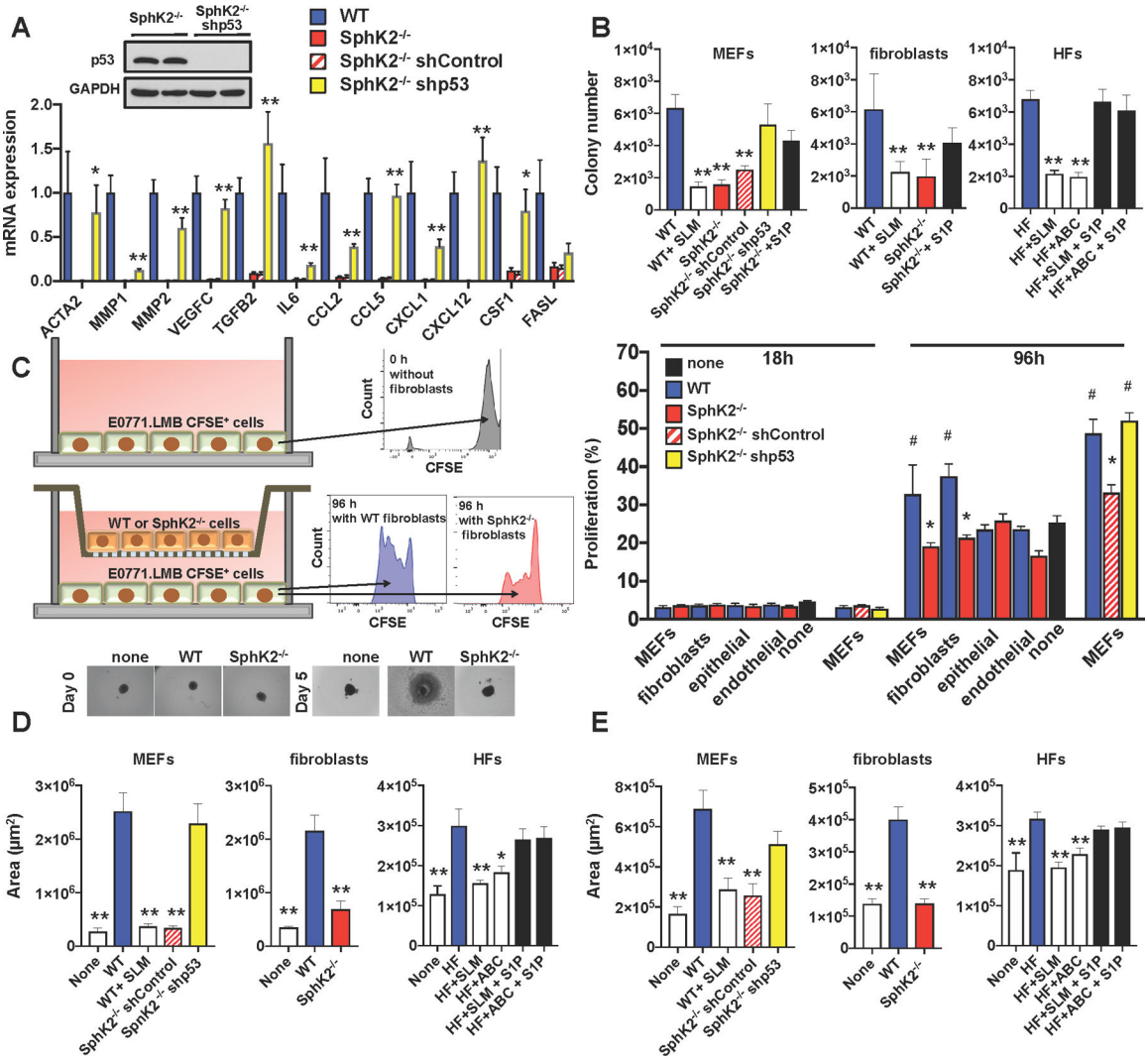

Figure 6. Repression of pro-tumorigenic factors in SphK2 knockout fibroblasts mediated by p53 attenuates breast cancer cell growth.

(A) Gene expressions were determined by QPCR in WT or SphK2 null MEFs or SphK2 null MEFs transduced with lentivirus expressing p53 shRNA (SphK2$^{-/-}$ shp53) or with control shRNA (SphK2$^{-/-}$ shControl). (n=6) Data are mean ± SEM. **p < 0.01 compared to shControl, Welch's t-test. Inset: Levels of p53 were examined by immunoblotting. (B) Conditioned medium (CM) from WT, SphK2$^{-/-}$ shControl, SphK2$^{-/-}$ shp53, or from primary lung fibroblasts from WT or SphK2$^{-/-}$ mice or from primary human mammary fibroblasts (HF) treated with 10 μM SLM6031434 (SLM), 10 μM ABC294640 (ABC), or additional 0.5 μM S1P as indicated was added to cultures of E0771.LMB cells and colony formation assessed by crystal violet staining and quantified. (n=5–10 in 3 independent experiments). Data are mean ± SD **p < 0.01 compared to WT or HF. One-way analysis of variance test followed by Dunnett's multiple comparisons test. (C) MEFs, primary lung fibroblasts, primary lung epithelial cells, and primary lung endothelial cells isolated from WT or SphK2$^{-/-}$ mice were cultured on the upper compartments of transwells containing CFSE-stained E0771.LMB cells in the lower compartment as illustrated. In

addition, WT, SphK2$^{-/-}$ shControl, or SphK2$^{-/-}$ shp53, were also cultured on the upper compartments. Percent proliferation of E0771.LMB cells was assessed after 18 h and 96 h by flow cytometry analysis. (n=3,5). Data are mean ± SEM. $^{\#}p < 0.05$ compared to none (without cells in the upper compartment). *p < 0.05 compared to appropriate WT. One-way analysis of variance test followed by Dunnett's multiple comparisons test, Welch's t-test. Representative flow cytometry analyses are shown in the upper panel. (D,E) CM from the indicated cells or control medium alone (None) treated as specified was added to E0771.LMB spheroids. (D) Representative pictures and quantitation of spheroid growth and (E) invasion into the extracellular matrix (n=6,12–14). Data are mean ± SEM from 2–3 independent experiments. *p < 0.05, **p < 0.01, compared to WT or HF. One-way analysis of variance test followed by Dunnett's multiple comparisons test.

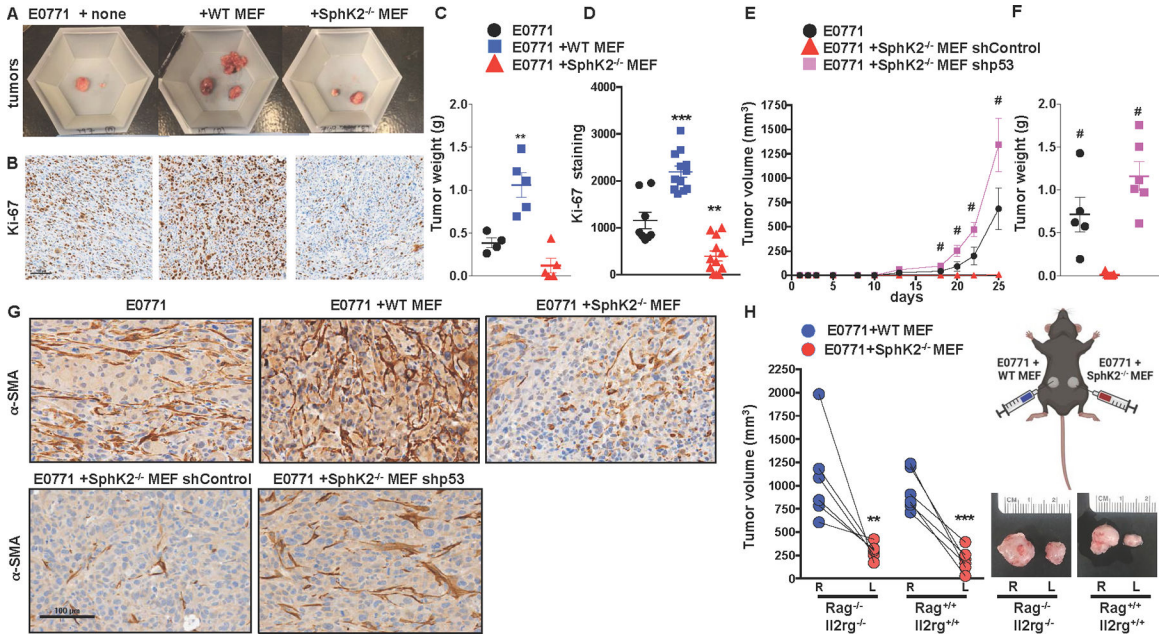

Figure 7. Loss of SphK2 in stromal fibroblasts suppresses breast cancer tumor growth.

(A-D) E0771.LMB cells were inoculated into bilateral 4th mammary pad, either alone or together with WT or SphK2$^{-/-}$ MEFs. Mice were sacrificed at day 25 (n=4,5 mice/group). (A) Representative tumors. (B) Representative Ki-67 staining. (C) Tumor weights. (D) Numbers of Ki-67 stained cells per field (n=8,12 different fields). (C,D) Data are mean ± SEM. **p < 0.01 compared to E0771 alone. One-way analysis of variance test followed by Dunnett's multiple comparisons test. (E,F) E0771.LMB cells were inoculated into bilateral 4th mammary pads, either alone or together with WT MEFs or together with SphK2$^{-/-}$ MEFs transduced with lentivirus expressing p53 shRNA (shp53) or shControl as indicated (n=5,7 mice/group). (E) Tumor volumes. (F) Tumor weights. Data are mean ± SEM. $^{\#}$p < 0.01 compared to E0771.LMB + SphK2$^{-/-}$ MEFs shControl. One-way analysis of variance test followed by Dunnett's multiple comparisons test. (G) Representative immunohistochemical staining of tumor sections for αSMA from the indicated mice group. Scale bar: 100 μm. (H) EO771.LMB (0.1×10^6) cells were co-injected with WT or SphK2$^{-/-}$ MEFs (0.1×10^6) into the left and right mammary fat pads of *Rag2*$^{-/-}$*Il2rg*$^{-/-}$ *mice,* respectively, as well as into the left and right mammary fat pads of control *Rag2*$^{+/+}$*Il2rg*$^{+/+}$ mice. Schematic of experimental design is shown. Tumor volumes were measured after 35 days, and representative images of tumors are shown. **p < 0.01, ***p < 0.001 compared left to right tumors. Unpaired two-tailed t-test.

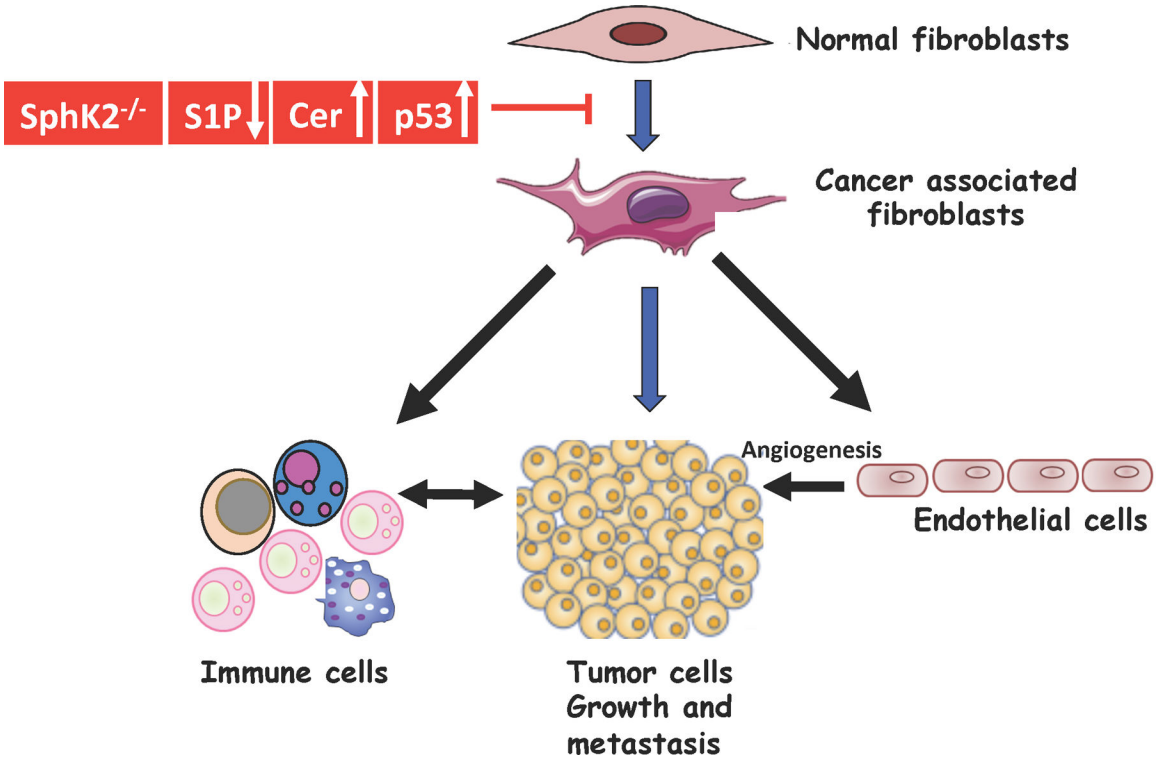

Figure 8. SphK2 and p53 axis regulates CAF secretome.

Deletion or inhibition of SphK2 leads to decreased S1P, increased ceramide, and stabilization of p53 in stromal fibroblasts. p53 acts in a non-cell autonomous manner to suppress their activation to CAFs, restraining their production of tumor-promoting factors and creating an active anti-tumor microenvironment. Blue arrows indicate the predominant mechanism.